Application of High-Order Discontinuous Galerkin Method to LES/DES Test Cases Using Computers with High Number of Cores

I. Bosnyakov[1,2], S. Mikhaylov[1,2], V. Podaruev[1,2],
A. Troshin[1,2] , V. Vlasenko[1,2] , A. Wolkov[1,2]

[1] Central Aerohydrodynamic Institute (TsAGI), Russia
[2] Moscow Institute of Physics and Technology (MIPT), Russia

Outline

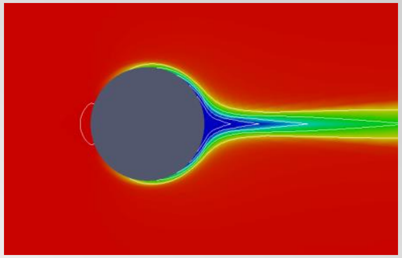

- Introduction
- Discontinuous Galerkin and Finite Volume methods
- Preliminary tests
  - Flow over cylinder
  - Evolution of 2D vortex

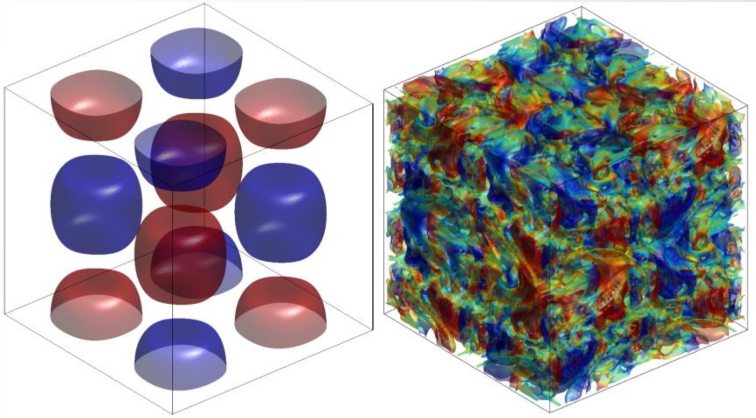

- Base tests
  - Taylor–Green vortex
  - Periodic hill flow
- Nozzle test case (first results)

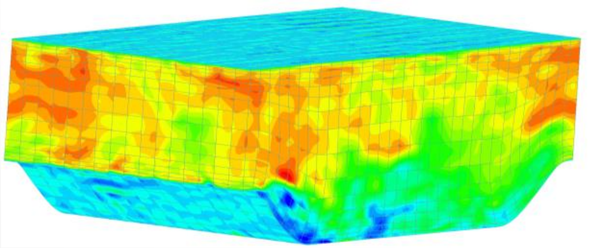

- Conclusions

Introduction

Towards Industrial LES/DNS in Aeronautics –

Paving the Way for Future Accurate CFD

- Objective: Development and testing of TsAGI code based on the high-order Discontinuous Galerkin Method (DG) for turbulent flow computations (aerodynamics, aeroacoustics)

- In addition, comparison with the Finite Volume Methods (FV – TsAGI's code) is presented

Finite Volume Method (implementation of TsAGI)

- Implementation of WENO is partial:
  - One-dimensional reconstruction
  - One quadrature point on the side of the cell
  - Central difference scheme for viscous terms

  $\boxed{\textbf{Class A, second order}}$ *)

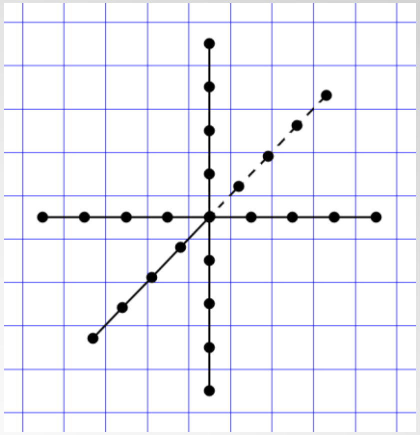

- In the following tests:
  - slope limiters are switched off (linear weights, no MP)
  - Roe Riemann solver is employed:

$$\mathbf{F}_{i+1/2} = \frac{1}{2}[\mathbf{F}(\mathbf{Q}_L) + \mathbf{F}(\mathbf{Q}_R)] - \frac{1}{2}\alpha(A^+ - A^-)(\mathbf{Q}_R - \mathbf{Q}_L);$$

$\alpha = 1 \rightarrow$ upwind scheme,
$\alpha = 0 \rightarrow$ central scheme

- Runge–Kutta, TVD3

*) Zhang R., Zhang M., Shu Ch. W. On the order of accuracy and numerical performance of two classes of finite volume WENO schemes // Communications in Computational Physics 9 (2011), No 3, pp. 807–827

Discontinuous Galerkin Method (1)

The system of equations and solution expansion:

$$\frac{\partial \mathrm{U}}{\partial t} + \nabla \cdot \mathbf{F}(\mathrm{U}, \mathbf{G}) = 0 \qquad \mathrm{U}(\mathbf{x}, t) = \sum_{j=1}^{K_f} \mathrm{u}_j(t)\varphi_j(\mathbf{x})$$

We multiply it by φ_i and integrate over the volume of cell Ω:

$$\int_\Omega \left(\frac{\partial \mathrm{U}}{\partial t} + \nabla \cdot \mathbf{F} \right) \varphi_i \, d\Omega = 0, \qquad i = 1, \ldots, K_f$$

Substituting the expansion of U and taking into account the orthonormality of basis functions,

$$\int_\Omega \varphi_i \varphi_j \, d\Omega = \delta_{ij}$$

We arrive at the equation system for expansion coefficients u_i :

$$\frac{d\mathrm{u}_i}{dt} + \oint_\Sigma \hat{\mathbf{F}} \cdot \mathbf{n} \, \varphi_i \, d\Sigma = \int_\Omega \mathbf{F} \cdot \nabla \varphi_i \, d\Omega$$

Discontinuous Galerkin Method (2)

The resulting system of equations:

$$\frac{d\mathrm{u}_i}{dt} + \oint_{\Sigma} \hat{\mathbf{F}} \cdot \mathbf{n}\, \varphi_i \, d\Sigma = \int_{\Omega} \mathbf{F} \cdot \nabla \varphi_i \, d\Omega$$

Roe Riemann solver for inviscid flux

Bassi–Rebay 2 method for viscous flux

- { $\boldsymbol{\varphi}_j$**(x)** } is full orthonormal polynomial set up to order *K=1, 2, 3, 4, 5*
- integration is performed using the Gauss formula with tensor product of 1D Gauss–Legendre quadratures
- second order curvilinear meshes are used
- Runge–Kutta, SSP5

Elementary hexahedrons and their mappings

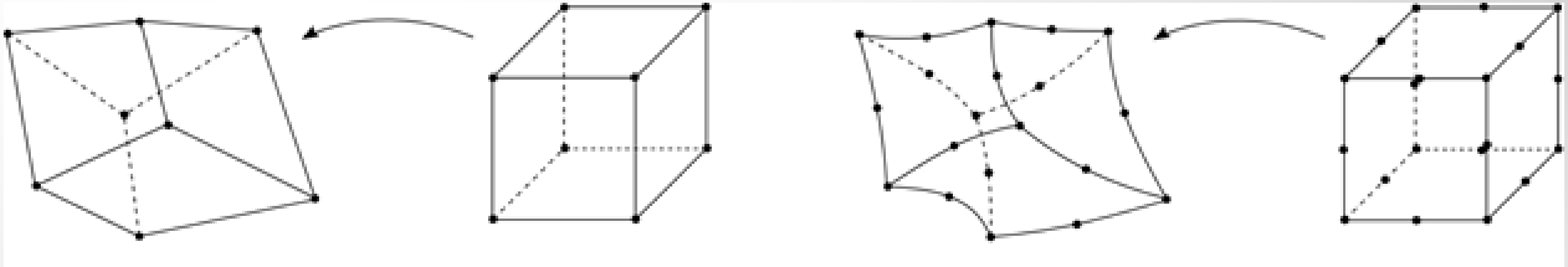

Serendipity transformations:
a) “linear”, 8 vertices

b) : “quadratic”, 20 points

Barycenter coordinates:

$$x_0 = \frac{\int_\Omega x d\Omega}{\int_\Omega d\Omega}, \quad y_0 = \frac{\int_\Omega y d\Omega}{\int_\Omega d\Omega}, \quad z_0 = \frac{\int_\Omega z d\Omega}{\int_\Omega d\Omega}$$

$$\mathbf{I} = \begin{bmatrix} \int_\Omega \left(\tilde{y}^2 + \tilde{z}^2\right) d\Omega & -\int_\Omega \tilde{x}\tilde{y}\, d\Omega & -\int_\Omega \tilde{x}\tilde{z}\, d\Omega \\ -\int_\Omega \tilde{x}\tilde{y}\, d\Omega & \int_\Omega \left(\tilde{x}^2 + \tilde{z}^2\right) d\Omega & -\int_\Omega \tilde{y}\tilde{z}\, d\Omega \\ -\int_\Omega \tilde{x}\tilde{z}\, d\Omega & -\int_\Omega \tilde{y}\tilde{z}\, d\Omega & \int_\Omega \left(\tilde{x}^2 + \tilde{y}^2\right) d\Omega \end{bmatrix}$$

symmetry and positive definiteness properties

$$\tilde{x} = x - x_0$$
$$\tilde{y} = y - y_0$$
$$\tilde{z} = z - z_0$$

Unit and mutually orthogonal eigenvectors of inertia tensor $\mathbf{I}$ is: $\mathbf{e}_1\ \mathbf{e}_2\ \mathbf{e}_3$

$$\begin{bmatrix} x_\Omega \\ y_\Omega \\ z_\Omega \end{bmatrix} = \begin{bmatrix} e_{11} & e_{12} & e_{13} \\ e_{21} & e_{22} & e_{23} \\ e_{31} & e_{32} & e_{33} \end{bmatrix} \begin{bmatrix} \tilde{x} \\ \tilde{y} \\ \tilde{z} \end{bmatrix}$$

Basis functions: $\psi_j(\mathbf{x}_\Omega) = s_j^{-1} x_\Omega^{\alpha_j} y_\Omega^{\beta_j} z_\Omega^{\gamma_j}, \quad \alpha_j, \beta_j, \gamma_j \in \mathbf{Z}_+, \quad 0 \le \alpha_j + \beta_j + \gamma_j \le K.$

$$s_j = \sqrt{\int_\Omega \left(x_\Omega^{\alpha_j} y_\Omega^{\beta_j} z_\Omega^{\gamma_j}\right)^2 d\Omega} \qquad \int_\Omega \psi_j^2(\mathbf{x}_\Omega) d\Omega = 1$$

- Introduction
- Discontinuous Galerkin and Finite Volume methods
- **Preliminary tests**
  - **Flow over cylinder**
  - Evolution of 2D vortex
- Base tests
  - Taylor–Green vortex
  - Periodic hill flow
- Nozzle test case (first results)
- Conclusions

Flow over cylinder: computational mesh and flow parameters

- A series of refined meshes with dimensions from 16 x 4 x 1 to 128 x 32 x 1 cells
- $R_{\text{cylinder}} = 0.5$, $R_{\text{outer}} = 20$, $\Delta z = 0.1$
- Cylinder surface is «slip wall», side planes are «symmetry»
- Freestream values are imposed at the outer boundary
- Freestream Mach number $M_\infty \approx 0.15$

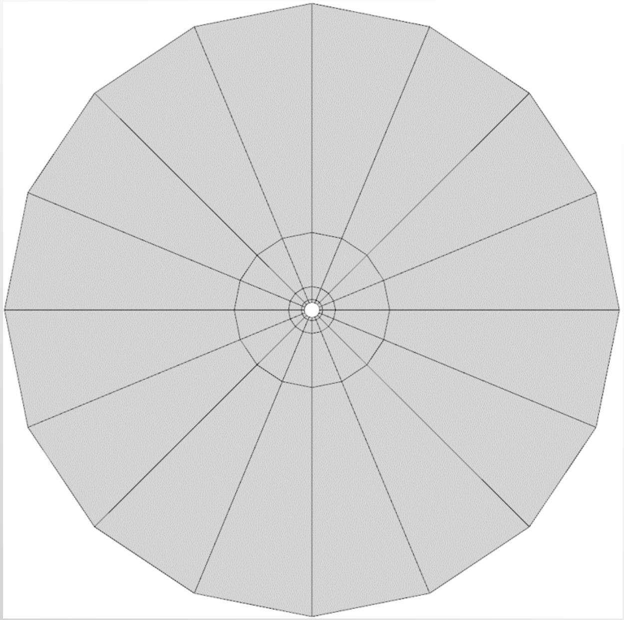

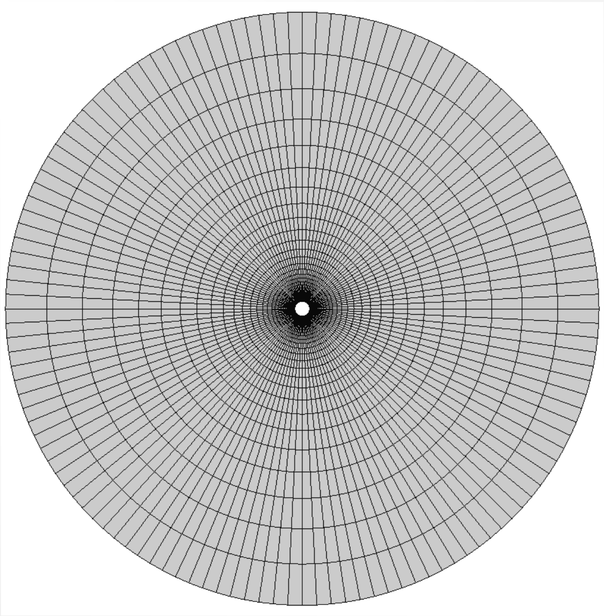

Flow over cylinder: total pressure field

- 128 x 32 x 1 mesh

polynomial order

FV, central scheme

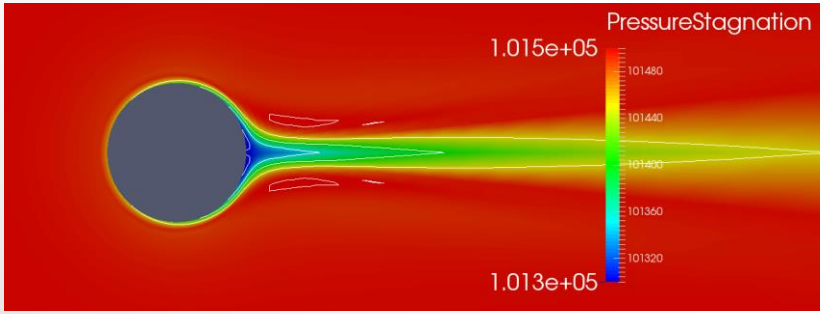

DG K = 1

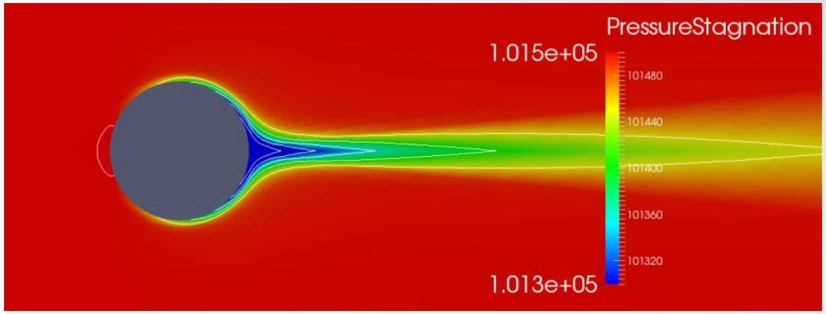

FV, WENO 5

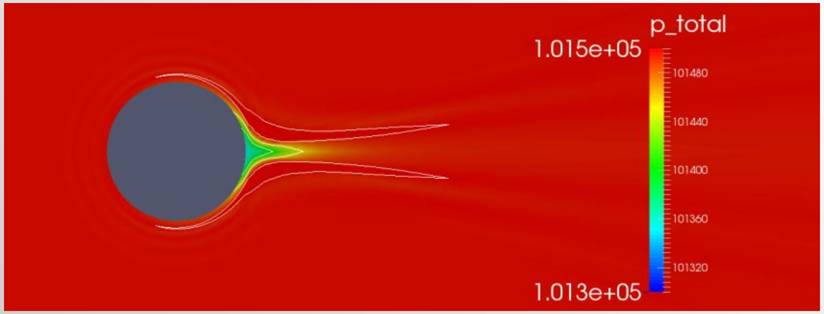

DG K = 3 on a curved mesh

Flow over cylinder: entropy error, L2 norm

$$e_{entropy} = \left(\frac{p}{p_\infty}\right) \Big/ \left(\frac{\rho}{\rho_\infty}\right)^{\kappa} - 1, \qquad Order = 2\,\frac{\log\left(e_{i-1} \,/\, e_i\right)}{\log\left(NDOF_i \,/\, NDOF_{i-1}\right)}.$$

NDOF = (Number of cells) x (Number of basis functions)

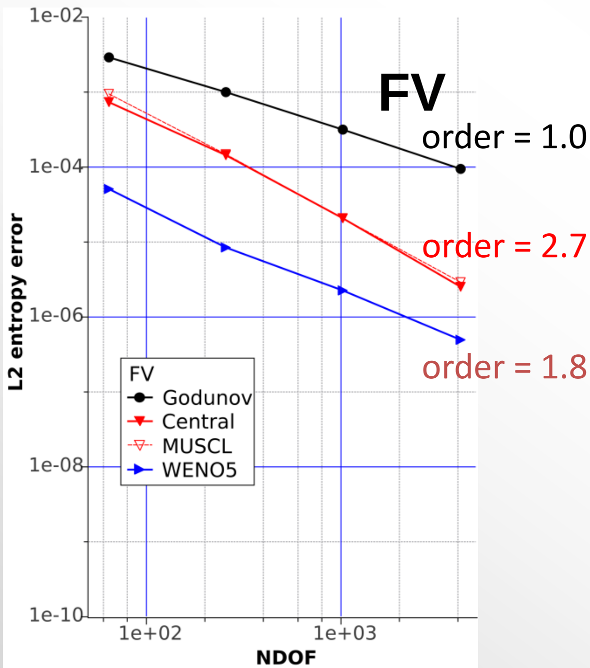

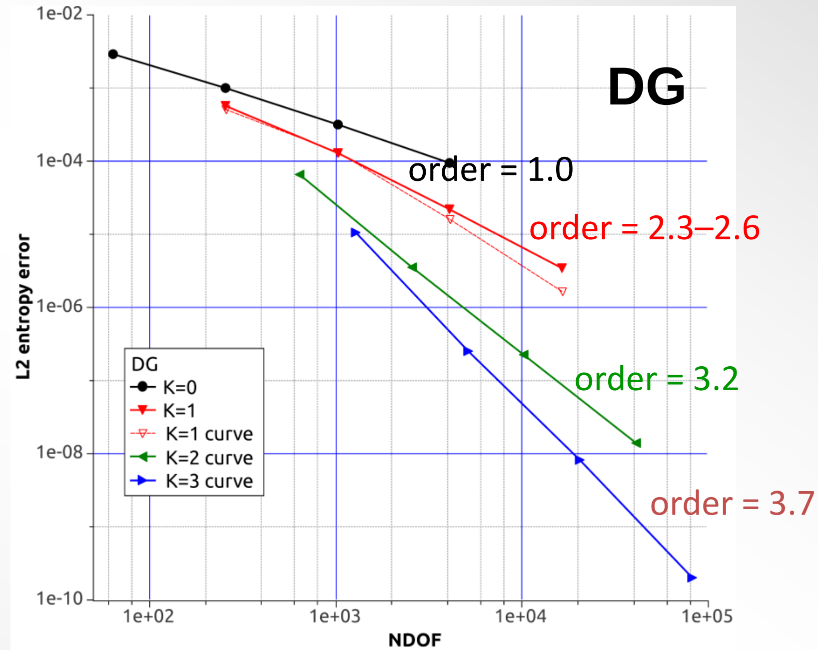

- With FV, error 10^{-10} can be achieved on a mesh of size 10^{10} DOFs
- DG requires only 10^5 DOFs for the same accuracy

- Introduction
- Discontinuous Galerkin and Finite Volume methods
- **Preliminary tests**
  - Flow over cylinder
  - **Evolution of 2D vortex**
- Base tests
  - Taylor–Green vortex
  - Periodic hill flow
- Nozzle test case (first results)
- Conclusions

Evolution of 2D vortex:

$$u = 1 - \frac{\varepsilon}{2\pi} e^{\frac{1}{2}\left(1-r^2\right)} y, \; v = 1 - \frac{\varepsilon}{2\pi} e^{\frac{1}{2}\left(1-r^2\right)} x,$$

$$T = 1 - \frac{(\gamma - 1)\varepsilon^2}{8\gamma\pi^2} e^{\left(1-r^2\right)}, \; \frac{p}{\rho^\gamma} = 1,$$

where $r^2 = x^2 + y^2, \; \varepsilon = 5$

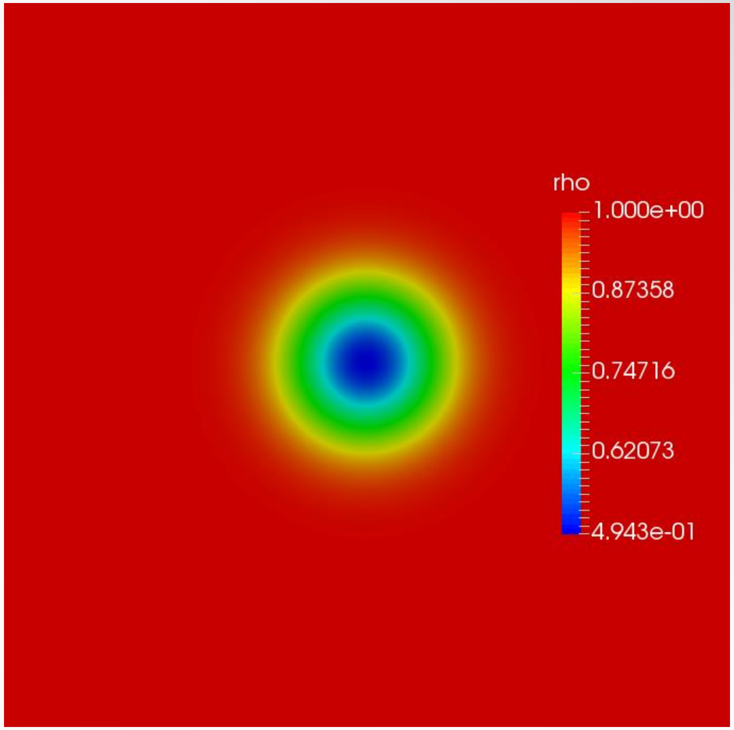

Evolution of 2D vortex: L0 error

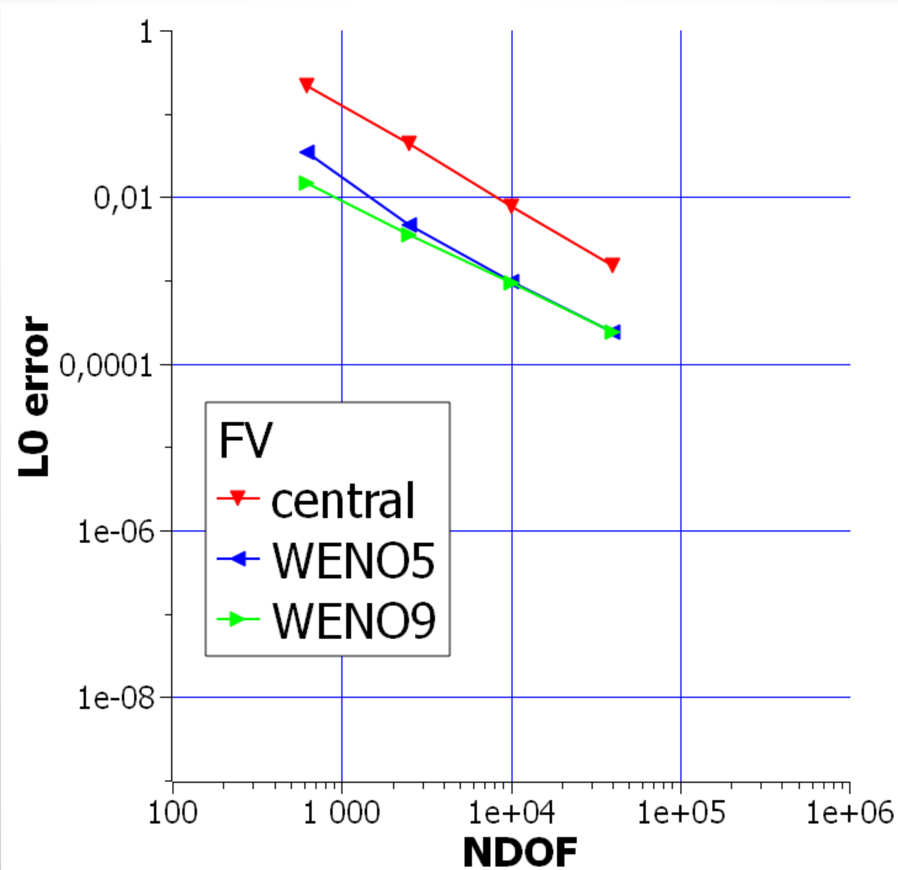

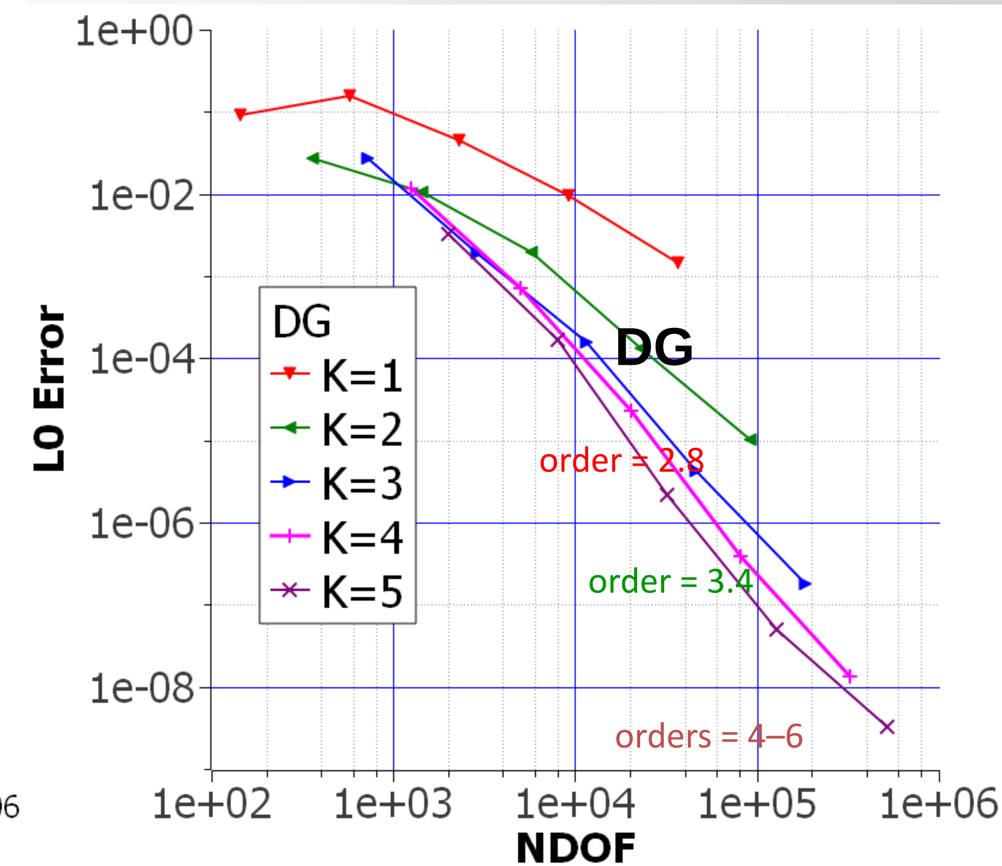

- With FV, error 10^{-8} can be achieved on a mesh of size 10^{10} DOFs
- DG requires only 10^{5} DOFs for the same accuracy

- Introduction
- Discontinuous Galerkin and Finite Volume methods
- Preliminary tests
  - Flow over cylinder
  - Evolution of 2D vortex
- **Base tests**
  - **Taylor–Green vortex**
  - Periodic hill flow
- Nozzle test case (first results)
- Conclusions

Taylor–Green Vortex test case

$$
\begin{aligned}
u &= V_0 \sin\left(\frac{x}{L}\right)\cos\left(\frac{y}{L}\right)\cos\left(\frac{z}{L}\right)\,, \\
v &= -V_0 \cos\left(\frac{x}{L}\right)\sin\left(\frac{y}{L}\right)\cos\left(\frac{z}{L}\right)\,, \\
w &= 0\,, \\
p &= p_0 + \frac{\rho_0 V_0^2}{16}\left(\cos\left(\frac{2x}{L}\right)+\cos\left(\frac{2y}{L}\right)\right)\left(\cos\left(\frac{2z}{L}\right)+2\right)
\end{aligned}
$$

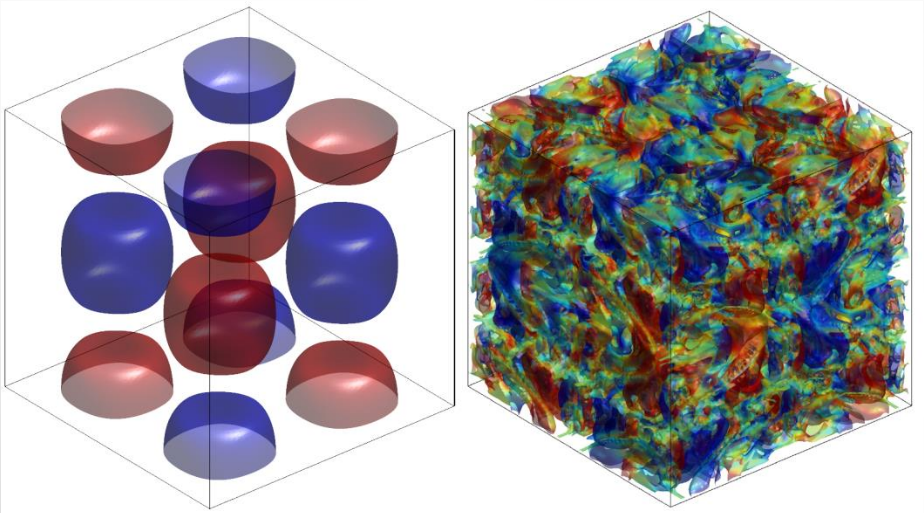

Pressure isosurfaces, Re = 1600

Taylor–Green Vortex: DG method accuracy, 64^3 mesh

Turbulent kinetic energy

$$E_k = \frac{1}{\rho_0 \Omega} \int_{\Omega} \rho \frac{v \cdot v}{2} d\Omega$$

Enstrophy

$$\epsilon = \frac{1}{\rho_0 \Omega} \int_{\Omega} \rho \frac{\omega \cdot \omega}{2} d\Omega$$

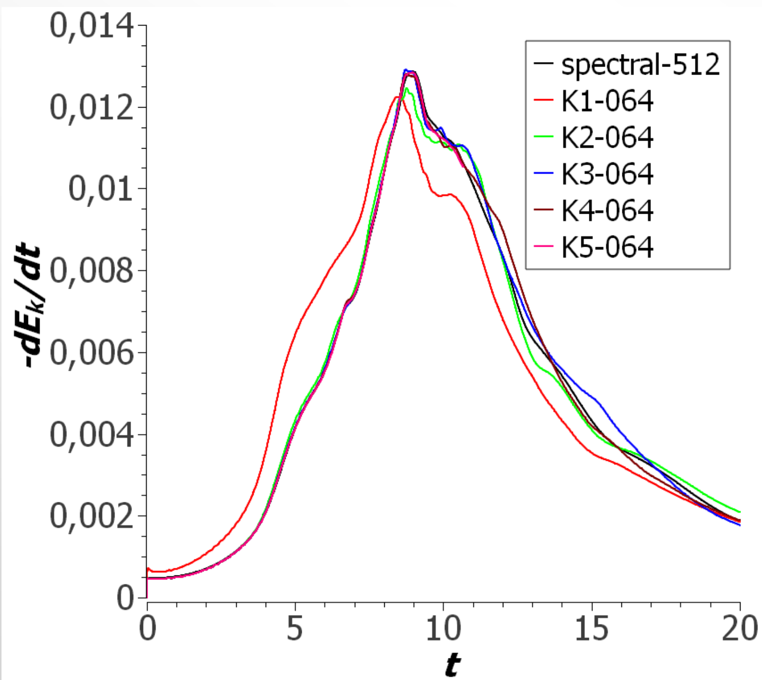

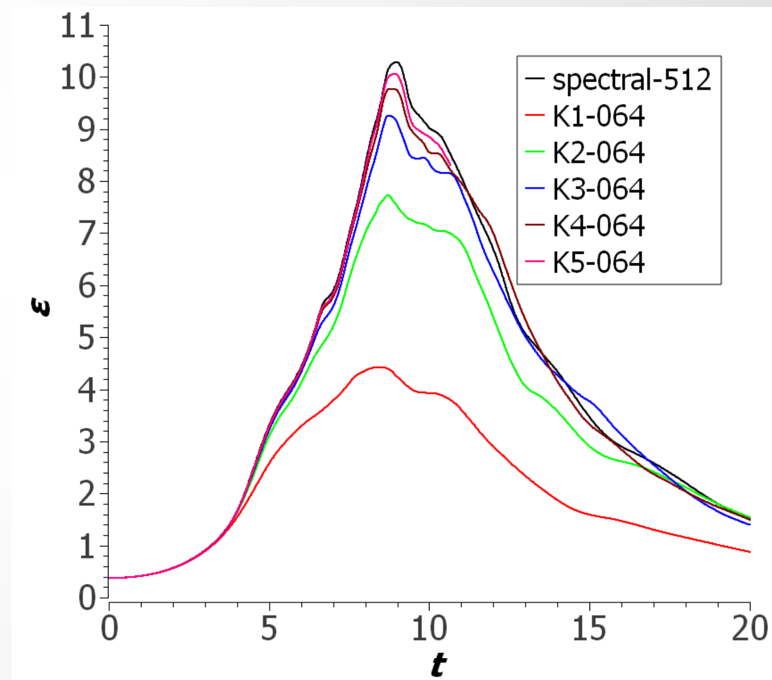

Spectral method reference data: W.M. van Rees, A. Leonard, D.I.Pullin, P. Koumoutsakos.
A comparison of vortex and pseudo-spectral methods for the simulation of periodic vortical flows at high Reynolds number // J. Comput. Phys. 230 (2011), pp. 2794–2805

Taylor–Green Vortex: convergence and time requirements

- NDOF = number of degrees of freedom
- t_{comp} = computing time for each calculation (scaled to 512 core cluster)
- error = enstrophy maximum difference obtained in the calculation and in the reference solution

FV schemes

	64^3	96^3	128^3	192^3	256^3	384^3	512^3
central			2.1×10^6 0.36 h 68%				
WENO5			2.1×10^6 0.49 h 45%				
WENO9	2.6×10^5 0.03 h 63%	8.8×10^5 0.13 h 50%	2.1×10^6 0.56 h 38%	7.1×10^6 2.3 h 23%	1.7×10^7 9.6 h 16%	5.7×10^7 39 h 8.0%	1.3×10^8 153 h 4.7%

DG schemes

	64^3	96^3	128^3
K = 1	1.0×10^6 0.23 h 60%	3.5×10^6 1.0 h 45%	8.4×10^6 3.7 h 37%
K = 2	2.6×10^6 1.8 h 25%	8.9×10^6 9.1 h 13%	2.1×10^7 32 h 6.9%
K = 3	5.2×10^6 10 h 10%	1.8×10^7 52 h 4.2%	4.2×10^7 159 h 2.2%
K = 4	9.2×10^6 39 h 5.0%	3.1×10^7 198 h 1.7%	7.3×10^7 623 h 0.89%
K = 5	1.5×10^7 136 h 2.2%		

- *Up to 4096 cores were used for DG computations*

Taylor–Green Vortex: enstrophy peak evaluation

$$\epsilon = \frac{1}{\rho_0 \Omega} \int_{\Omega} \rho \frac{\omega \cdot \omega}{2} d\Omega$$

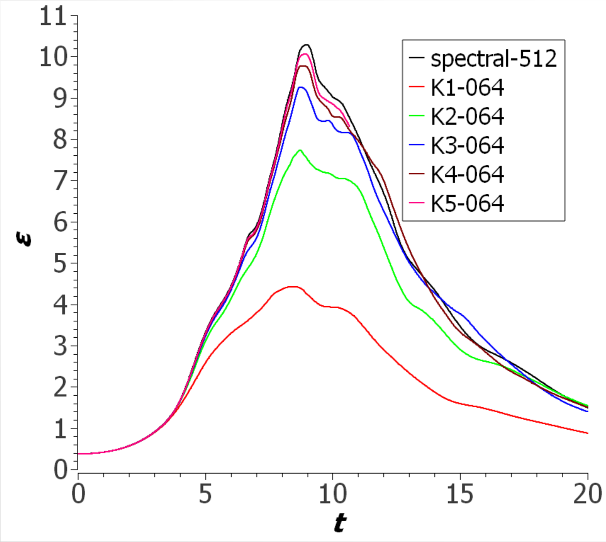

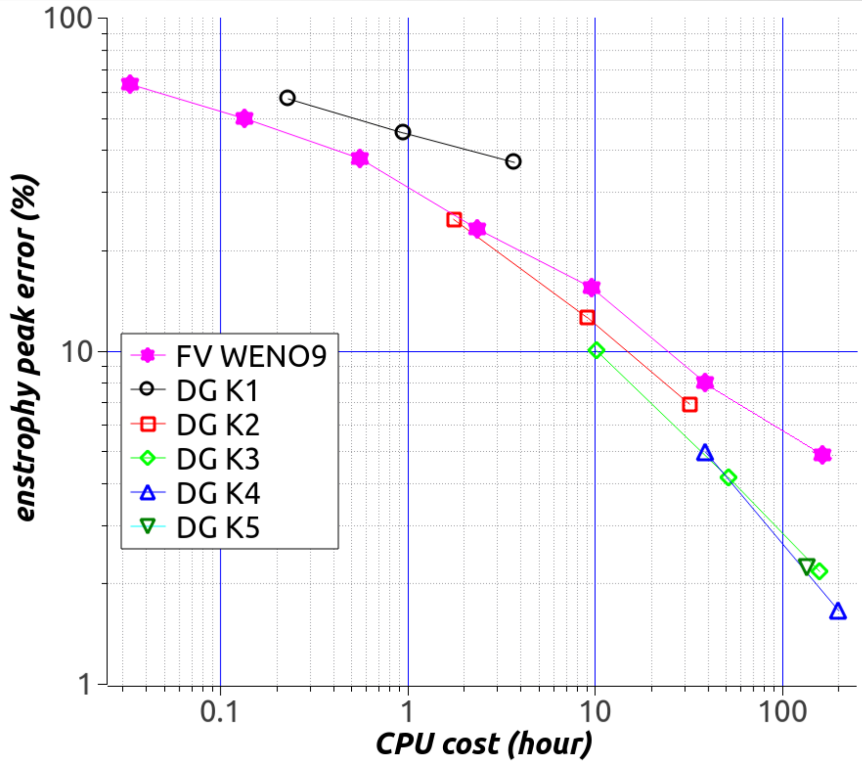

After K>2 increase in the order of the scheme and increase in the computational grid size have virtually equal effect on enstrophy error level

Taylor–Green Vortex: MPI scalability

- max – maximum possible acceleration (max = N_{cores})
- opt – acceleration 1.8 times for every doubling of CPU cores

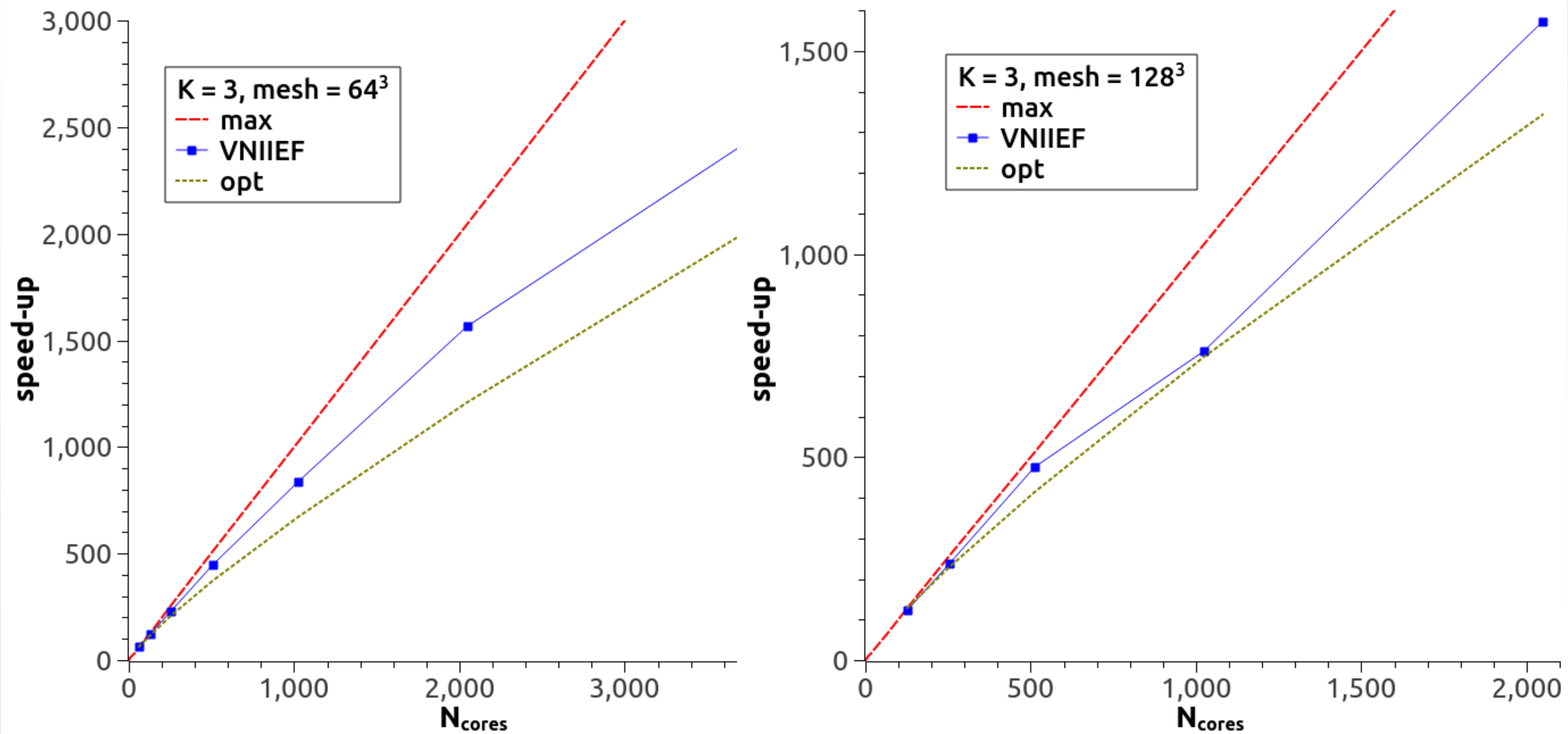

Increase in the number of cores (> 4,000) leads to reduction in scalability

Taylor–Green Vortex: OpenMP scalability

MPI - Separated memory for each core and a big data exchanges;
OpenMP - Shared memory for all cores of the computer node;

TsAGI cluster: 32 CPU cores on each computer node -> 8 CPU cores can be joint into one 8-thread process without loss of computational efficiency

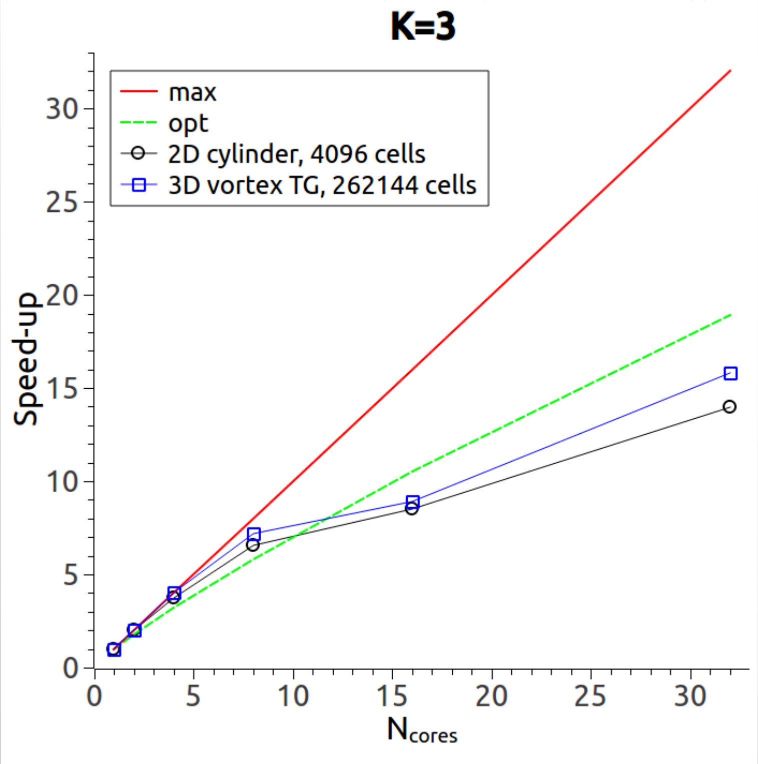

forecast:

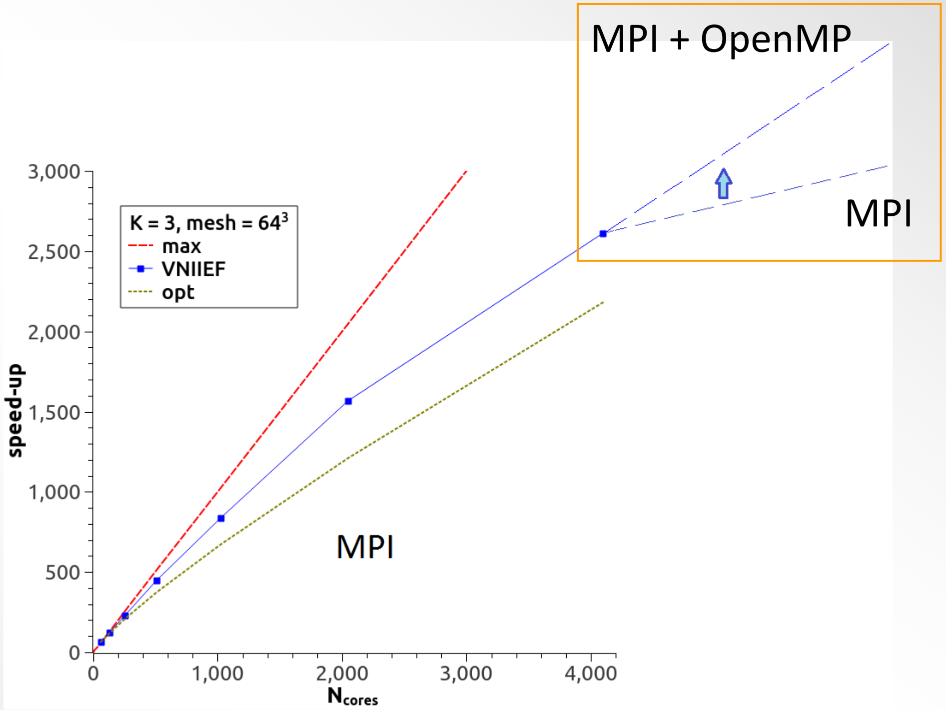

- MPI + OpenMP approach is promising with further increase of core number

- Introduction
- Discontinuous Galerkin and Finite Volume methods
- Preliminary tests
  - Flow over cylinder
  - Evolution of 2D vortex
- **Base tests**
  - Taylor–Green vortex
  - **Periodic hill flow**
- Nozzle test case (first results)
- Conclusions

Periodic hill flow

- An ERCOFTAC QNET CFD UFR 3-30 test case

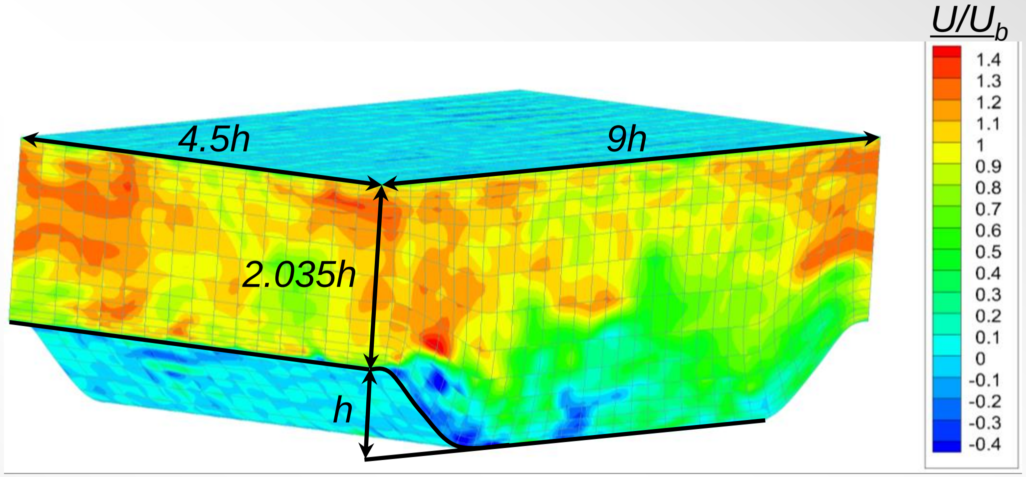

- streamwise and spanwise periodic flow
- forcing term dp/dx is imposed to maintain the mass flow rate
- Reynolds number Re = 10595, Mach number M ≈ 0.1
- uniform initial flowfield, initial state is “forgotten”
- Implicit Large Eddy Simulation (ILES) based on DG K = 1, 2, 3

Periodic hill flow: computational mesh and averaging

relatively coarse 32 x 16 x 16 mesh has been used

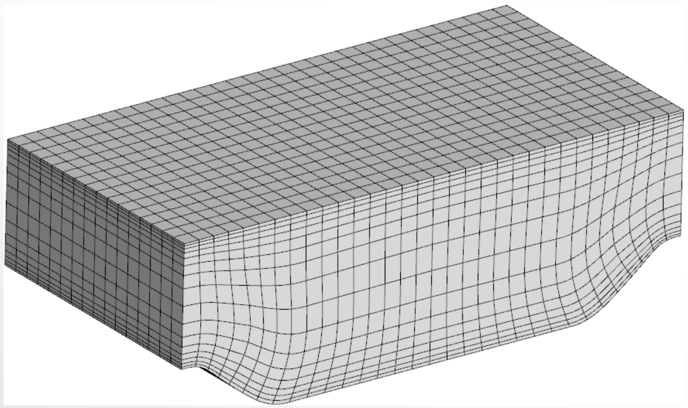

Averaging method

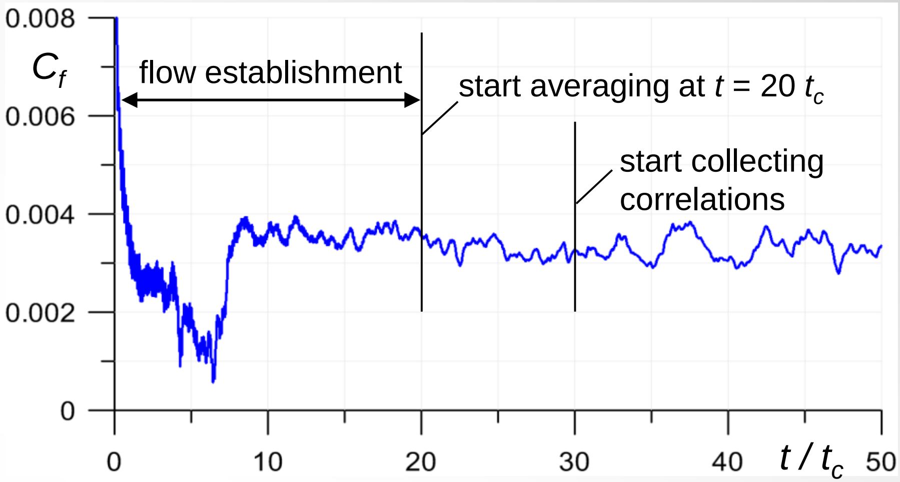

- The following data are collected:
  - Average velocity, pressure, density fields $U, V, W, P, \overline{\rho}$
  - Correlations (at the moment, in cell centers only $\overline{u'^2} = \overline{(u-U)^2},\ \overline{v'^2}, \overline{w'^2},\ \overline{u'v'}, \overline{u'w'}, \overline{v'w'}$
- Averaging is done over time (for at least 15 t_c) and over span (z axis direction)

Reference solution: NDOF = 13,100,000;
DG solution: K=1 – NDOF=32*16*16*4=32,768
K=2 81,920
K=3 163,840

Periodic hill flow: mean velocity profiles

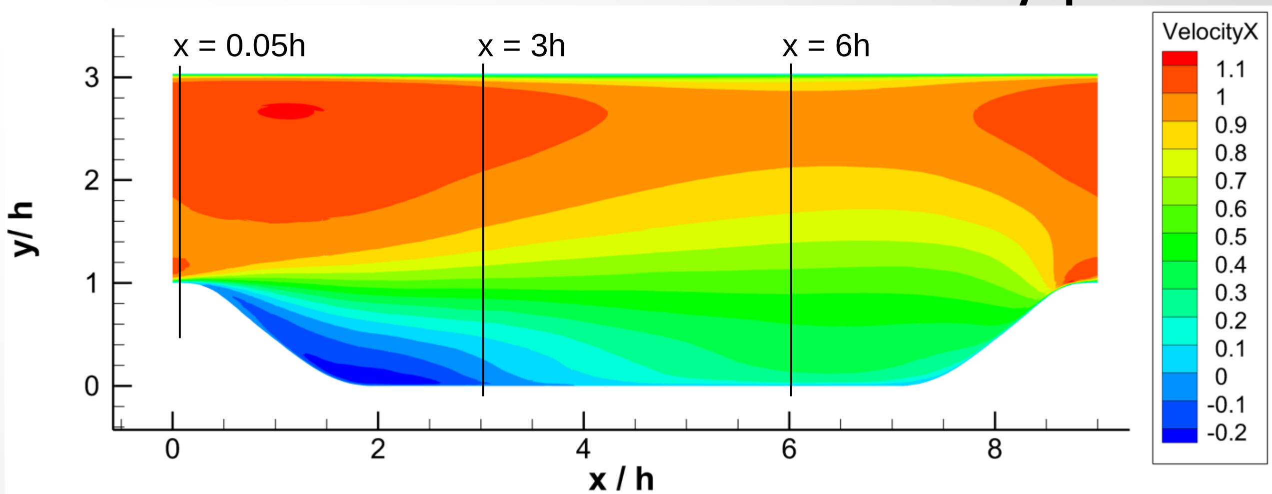

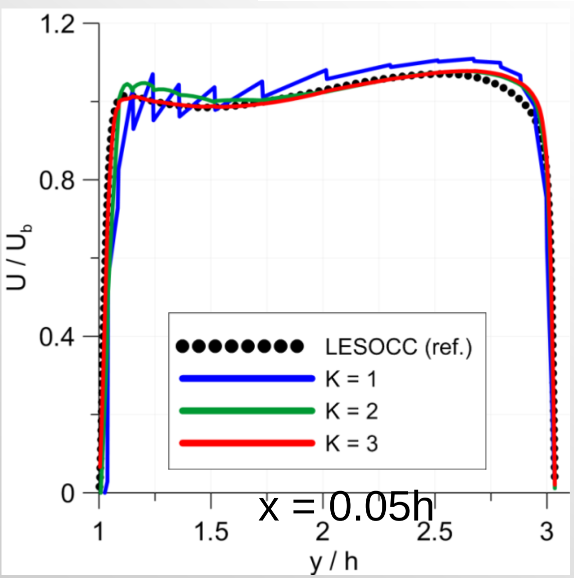

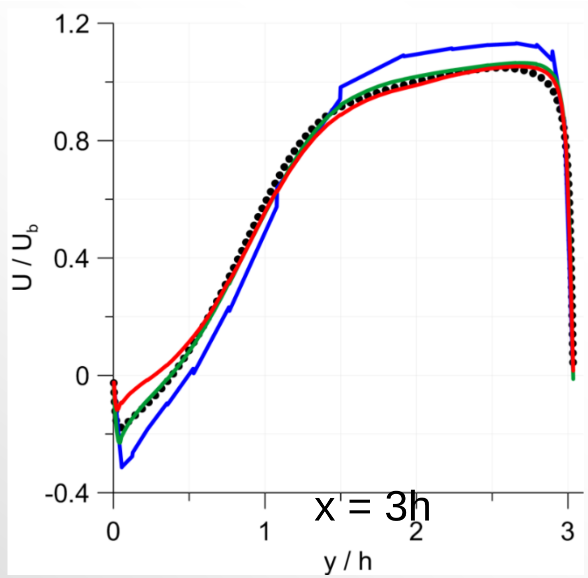

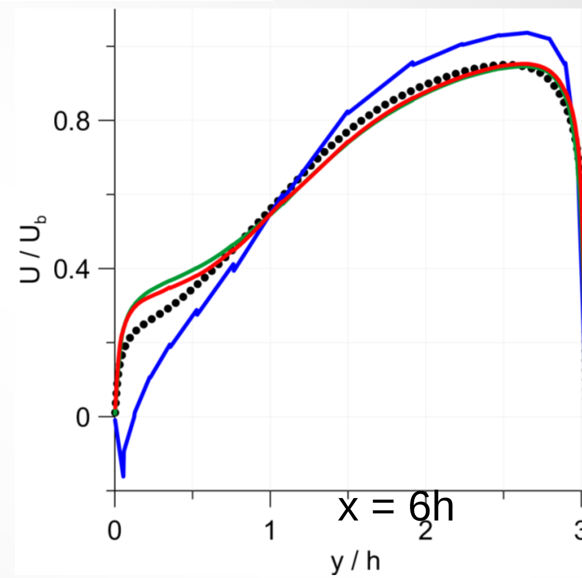

- Reference LES data: M. Breuer, N. Peller, Ch. Rapp, M. Manhart, Comput. Fluids 2009

Periodic hill flow: shear stress profiles

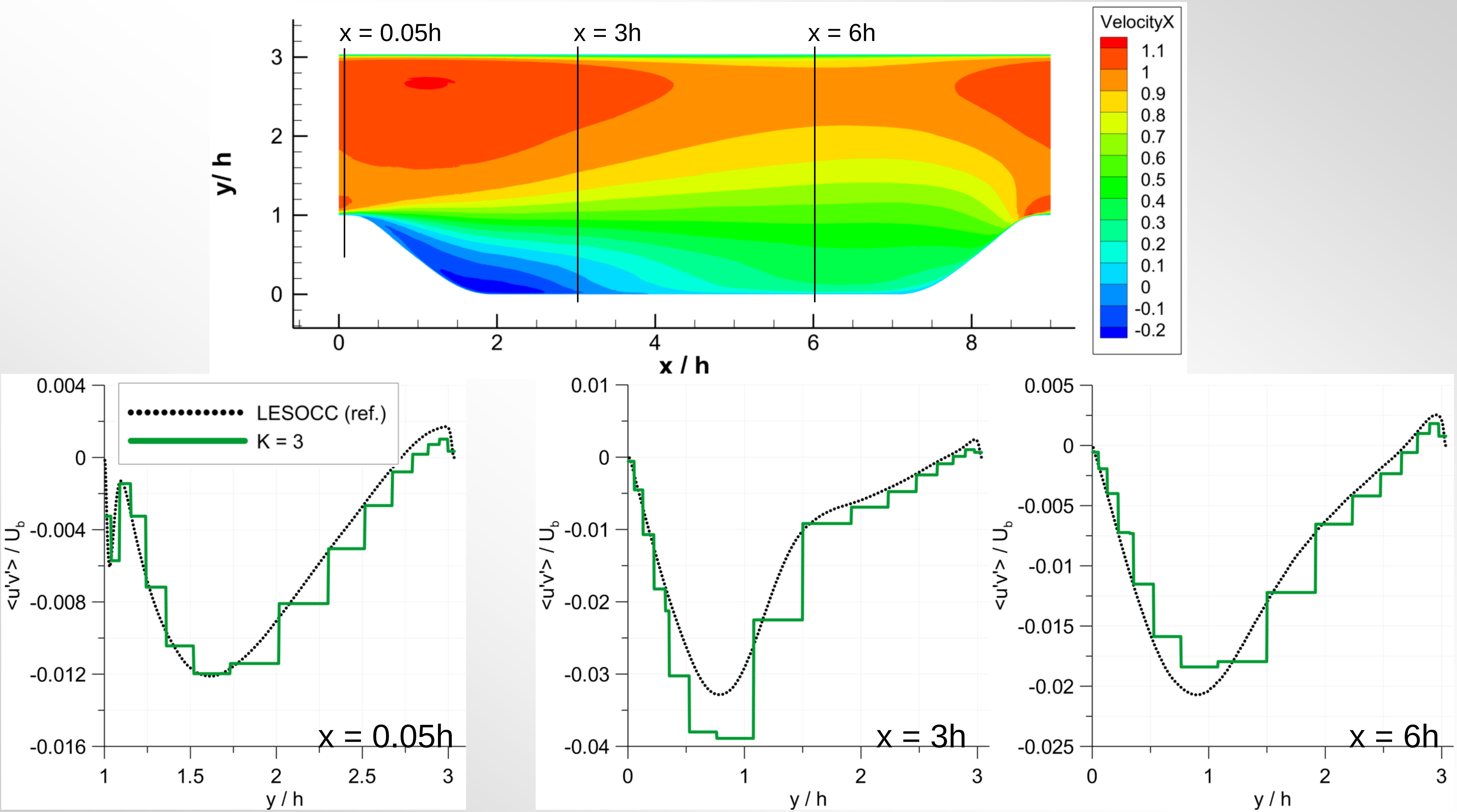

- Reference LES data: M. Breuer, N. Peller, Ch. Rapp, M. Manhart, Comput. Fluids 2009

- Introduction
- Discontinuous Galerkin and Finite Volume methods
- Preliminary tests
  - Flow over cylinder
  - Evolution of 2D vortex
- **Base tests**
  - Taylor–Green vortex
  - Periodic hill flow (first results)

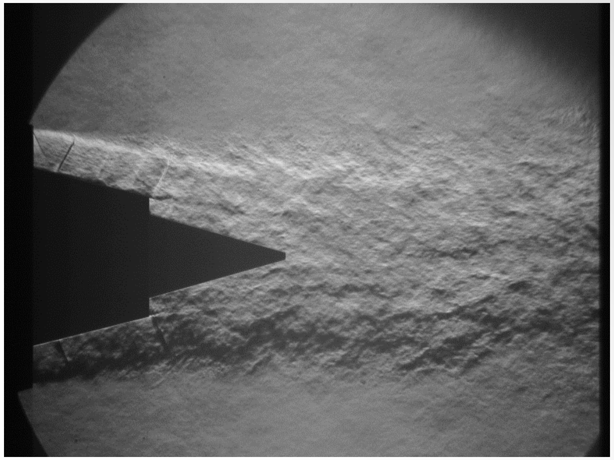

- **Nozzle test case (first results)**
- Conclusions

Detached-eddy Simulation DDES

P.R. Spalart, S. Deck, M.L. Shur, K.D. Squires, M.Kh. Strelets, A. Travin. A new version of detached-eddy simulation, resistant to ambiguous grid densities // Theor. Comput. Fluid Dyn. **20**, pp. 181–195, 2006

- A modified SA equation of the turbulence model is solved :

$$\frac{\partial \tilde{\nu}}{\partial t} + u_j \frac{\partial \tilde{\nu}}{\partial x_j} - \frac{\partial}{\partial x_j}\left(\frac{\nu + \tilde{\nu}}{\mathrm{Pr}_t^{\tilde{\nu}}} \frac{\partial \tilde{\nu}}{\partial x_j} \right) = P_{\tilde{\nu}}(\ldots, \boxed{\tilde{d}}) - D_{\tilde{\nu}}(\ldots, \boxed{\tilde{d}})$$

- The length scale varies smoothly from d_{wall} (RANS) to Δ_{cell} (LES):

$$\tilde{d} = d_{\mathrm{wall}} - f_d \max\left(0, d_{\mathrm{wall}} - C_{\mathrm{DES}} \Delta_{\mathrm{cell}}\right)$$

$$f_d = 1 - \mathrm{th}\,(8 r_d)^3$$

$$r_d = \frac{\nu + \nu_t}{\sqrt{\frac{\partial u_i}{\partial x_j}\frac{\partial u_i}{\partial x_j}}\,\mathrm{K}^2 d_{\mathrm{wall}}^2}$$

$$\Delta = \max\left(h_x, h_y, h_z\right)$$

$$C_{\mathrm{DES}} = 0.65, \ \mathrm{K} = 0.41$$

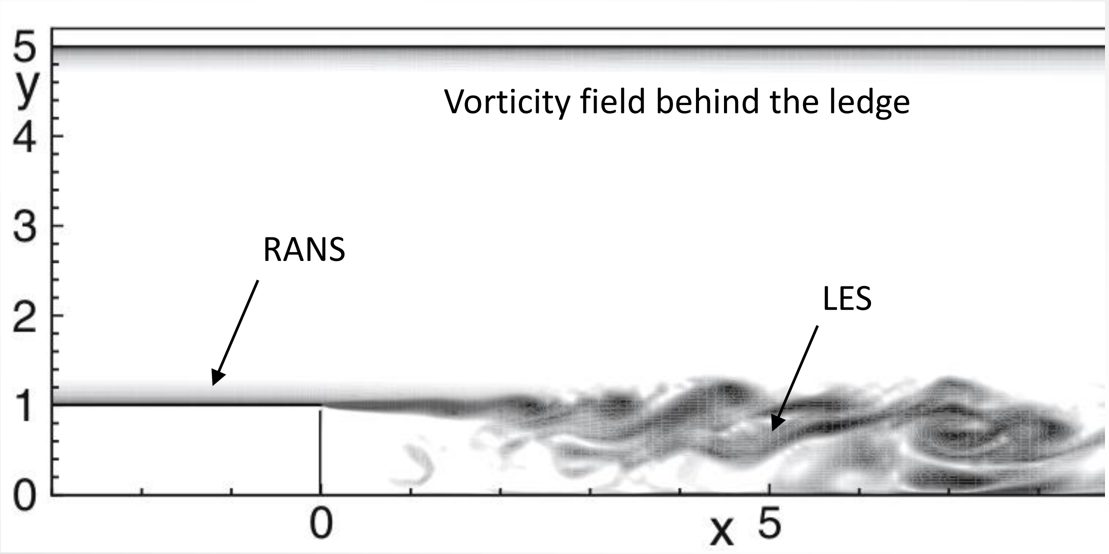

“Noise suppressing nozzle” test case TC-P4: Dual-stream jet nozzle

front view

- dual-stream coaxial nozzle
- cental body
- cold air flow
- pressure difference between the contours is generated by the grids

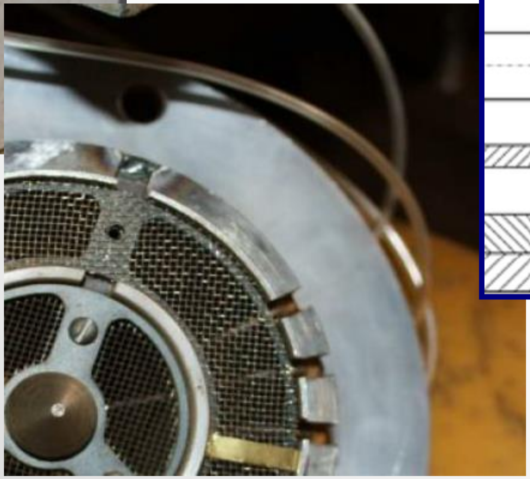

back view

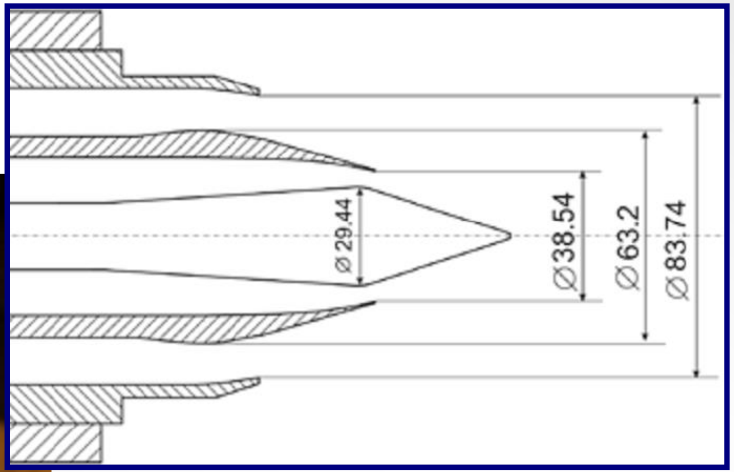

Flow regime and visualization

Inner contour:

- subsonic jet, M = 0.85 at nozzle exit
- nozzle pressure ratio $NPR_1 = 1.72$
- diameter-based Reynolds number $Re_{1D} = 0.96 \cdot 10^6$

Outer contour:

- supersonic underexpaneded jet, M=1 at nozzle exit
- nozzle pressure ratio $NPR_2 = 2.25$
- diameter-based Reynolds number $Re_{2D} = 2.872 \cdot 10^6$

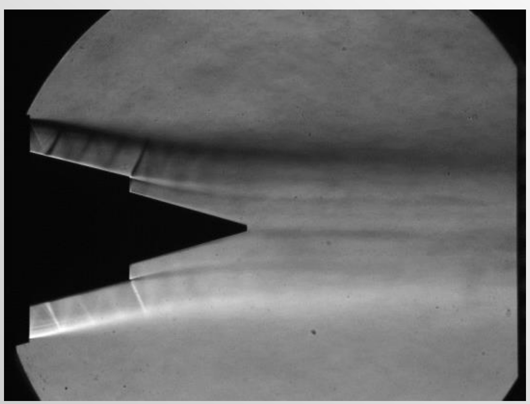

Shlieren visualization,
0.01 s exposure

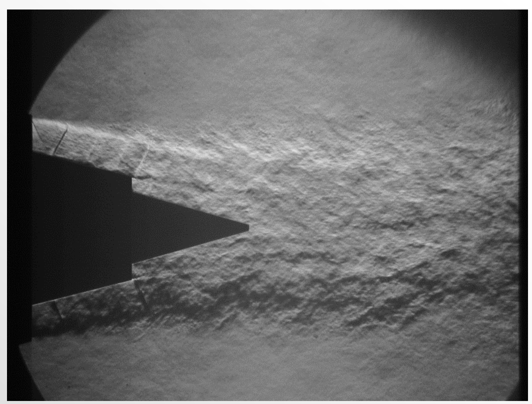

Shlieren visualization,
$3 \cdot 10^{-6}$ s exposure

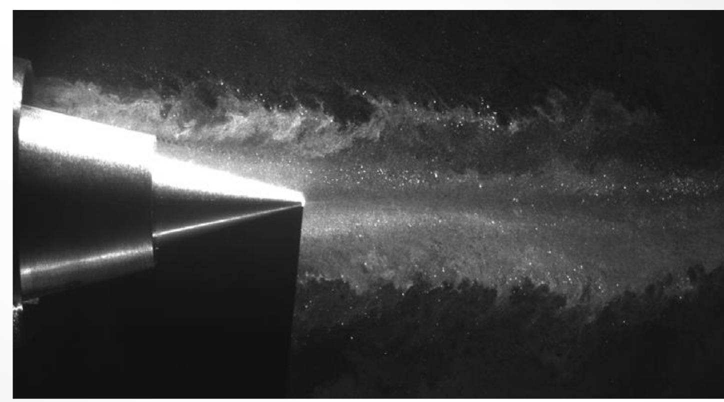

Laser knife visualization

Pitot pressure measurements

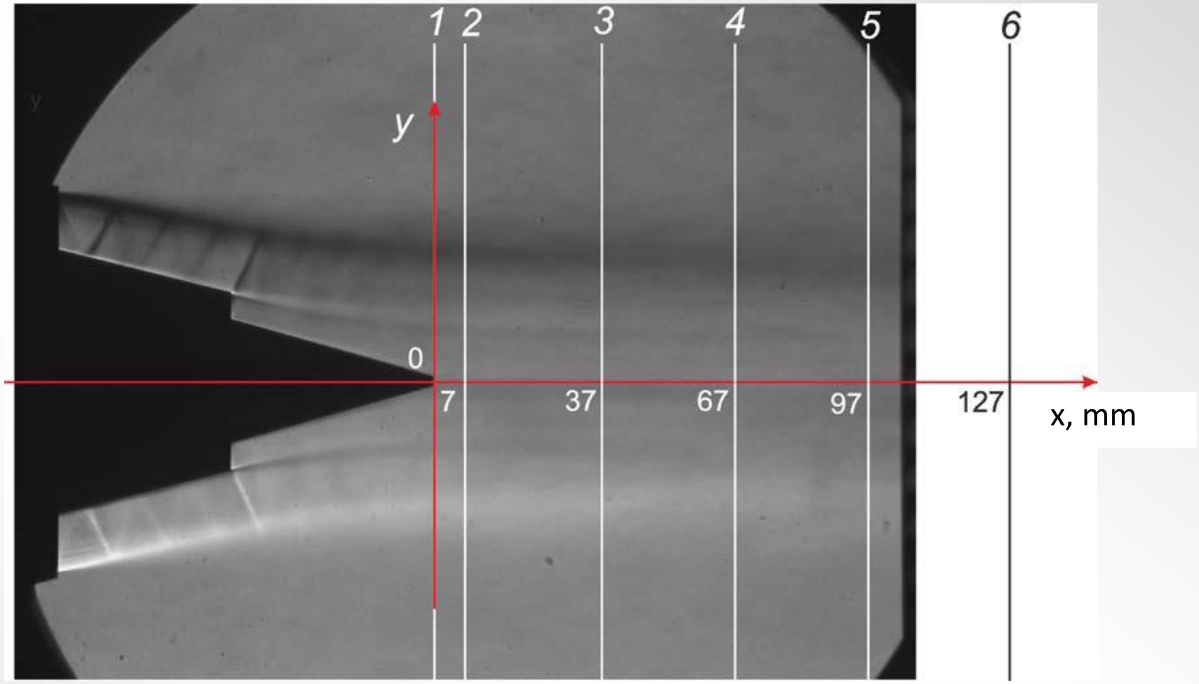

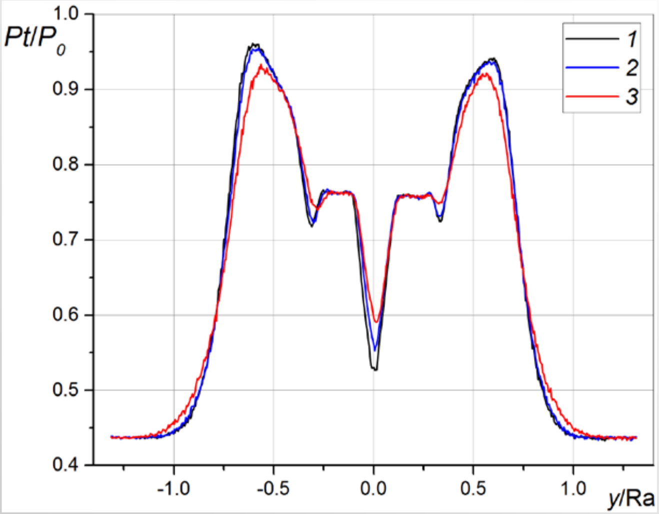

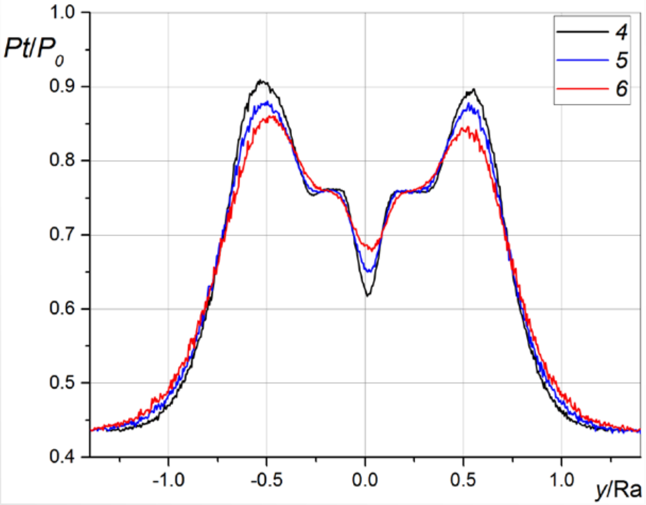

Root mean square mass flow rate pulsations at different jet cross sections and frequency amplitude spectrum was observed using hot wire

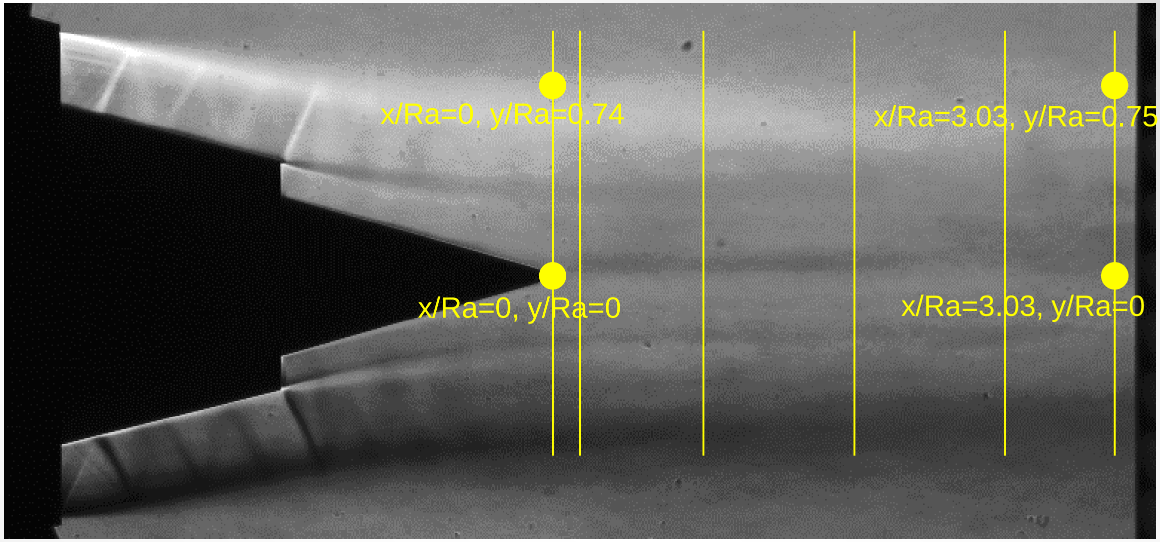

$$\langle m' \rangle = \frac{(\rho U)'}{\overline{\rho U}}$$

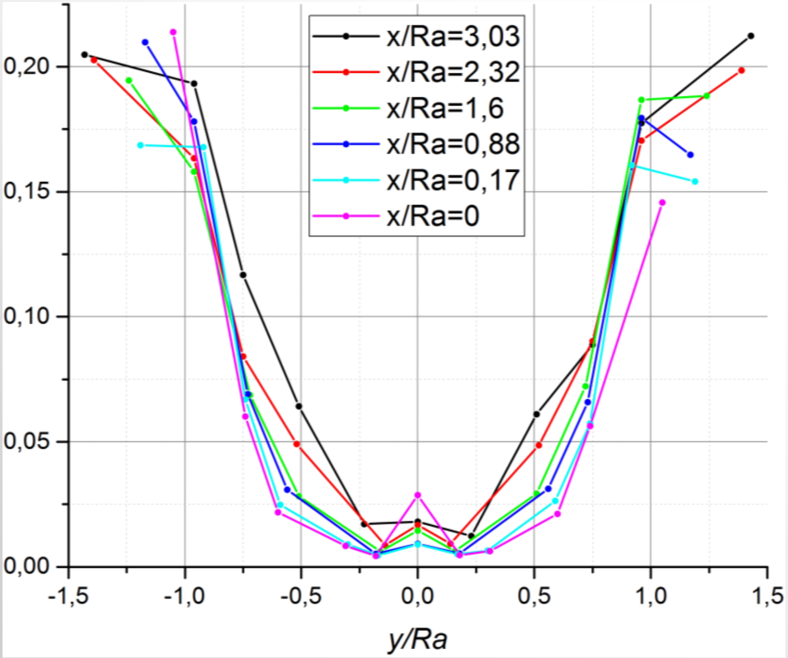

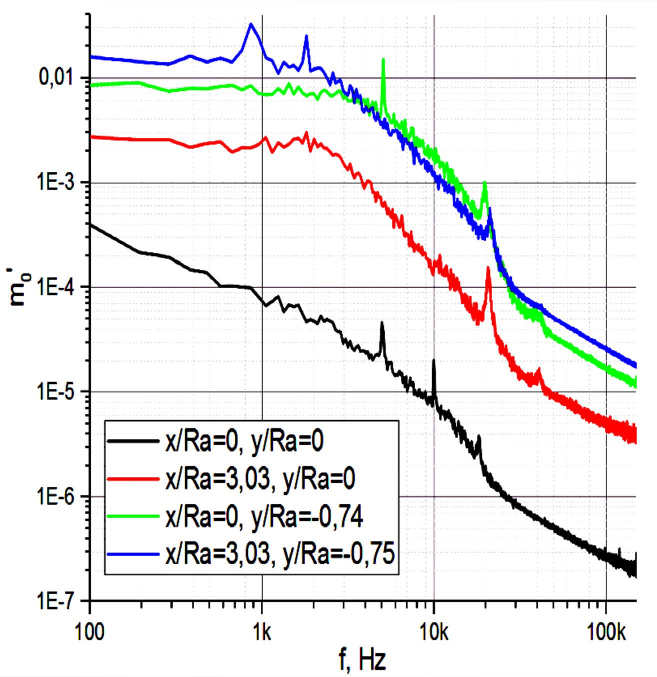

Meshes for finite volume computations

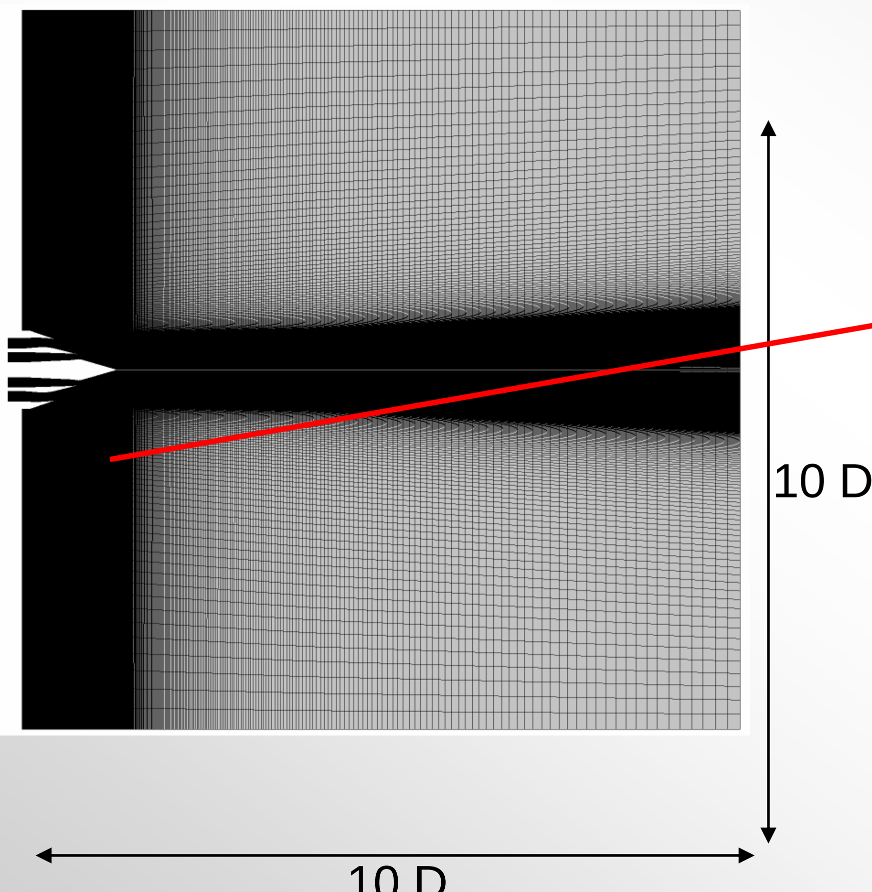

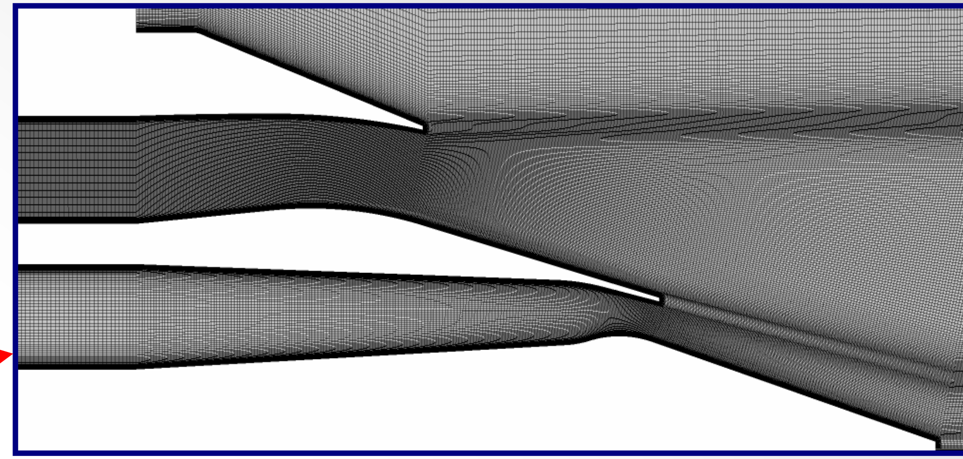

- 3D hexahedral structured mesh, $25 \cdot 10^6$ cells
- Initial steady RANS computation using SST turbulence model
- RANS flowfield used as initial conditions for unsteady DES-SST computation
- 140 characteristic times have been simulated

- Free outer boundaries with supersonic outlet
- Smooth adiabatic no-slip nozzle walls
- Inlet with uniform flow in the contours, Tu=1% (outer contour) and 10% (inner contour; decays quickly within the nozzle)

Flowfields obtained in computations

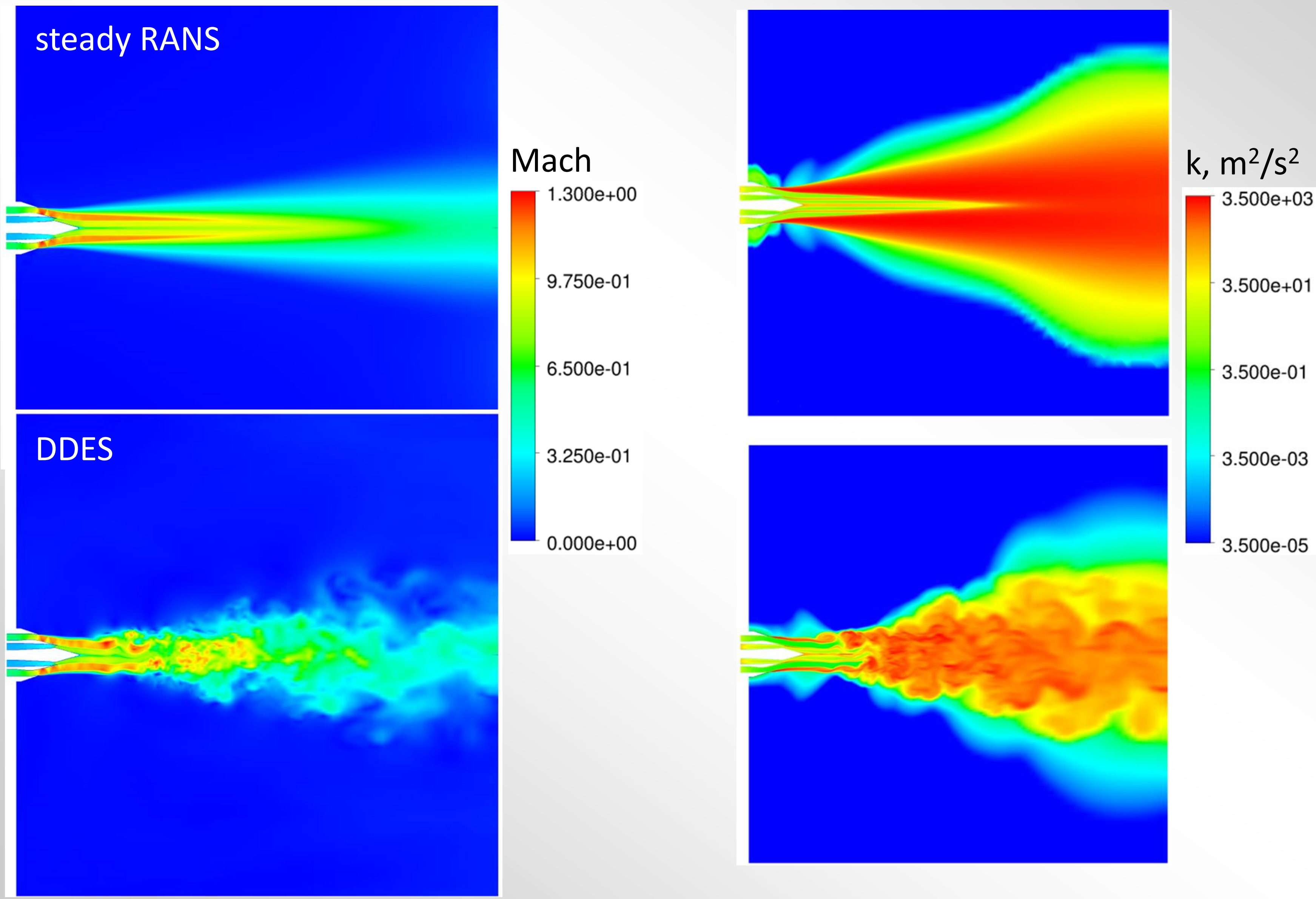

RANS computation results: pressure profiles

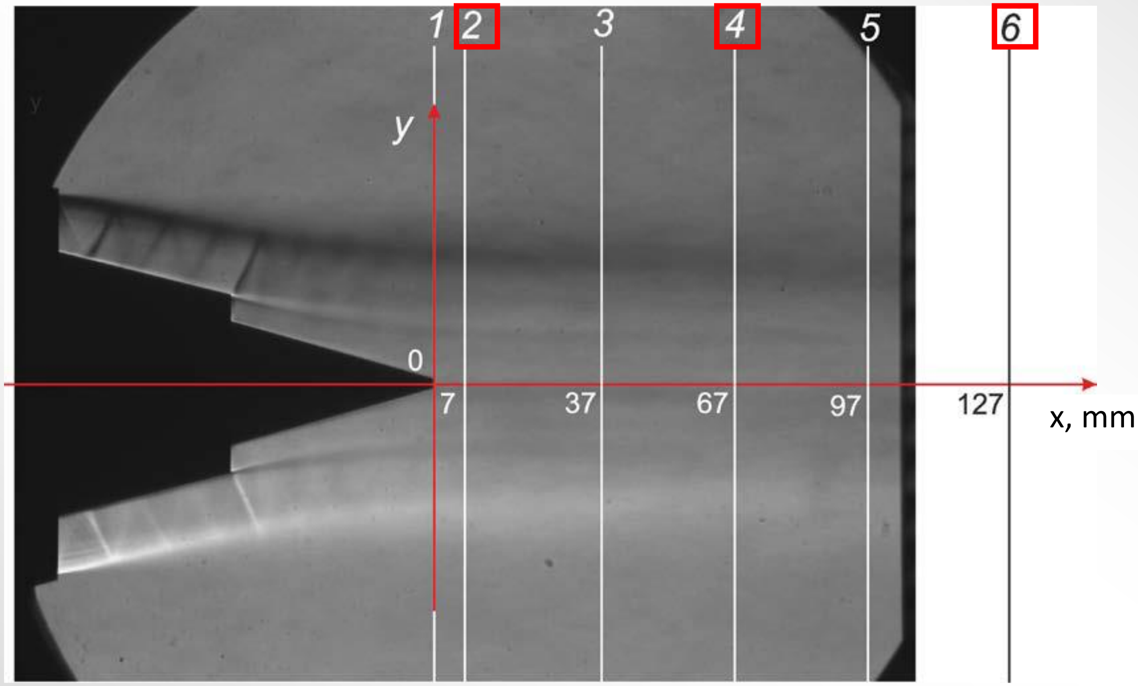

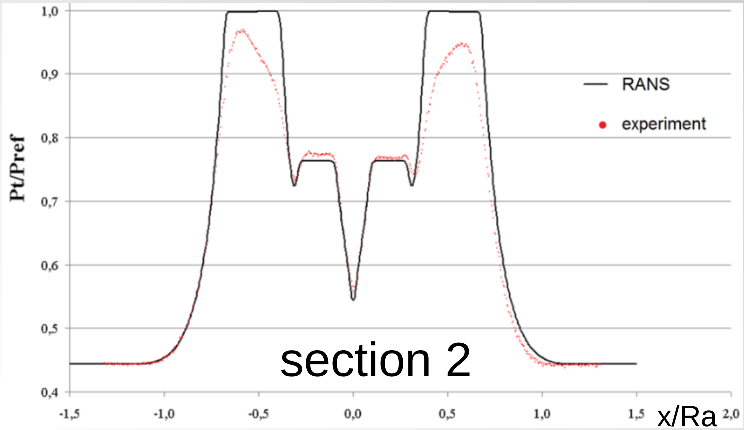

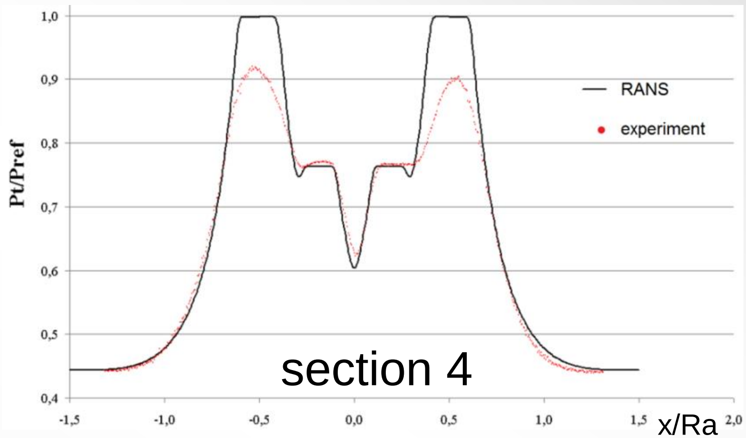

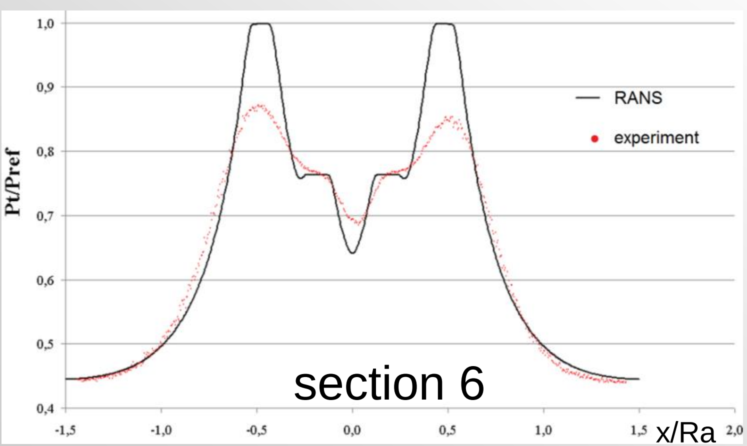

- boundary layers in outer contour are too thin in the computation
- wake diffusion behind the central body is underpredicted
- outer mixing layer growth rate is captured well

DES computation results: mass flow rate spectra

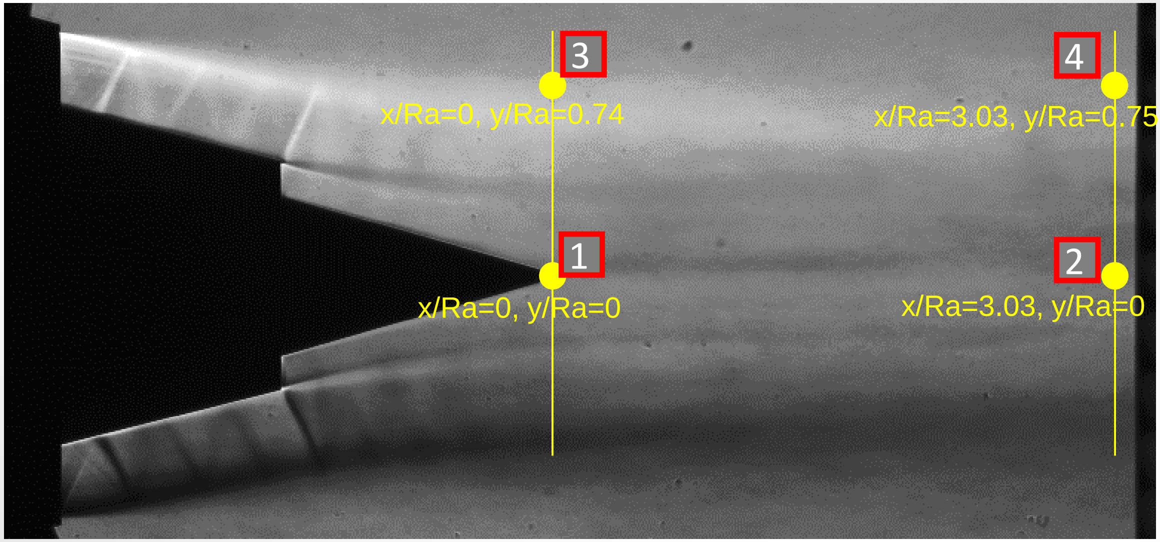

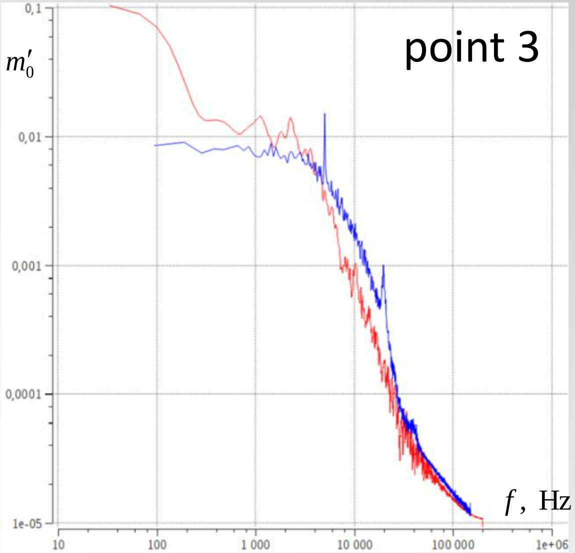

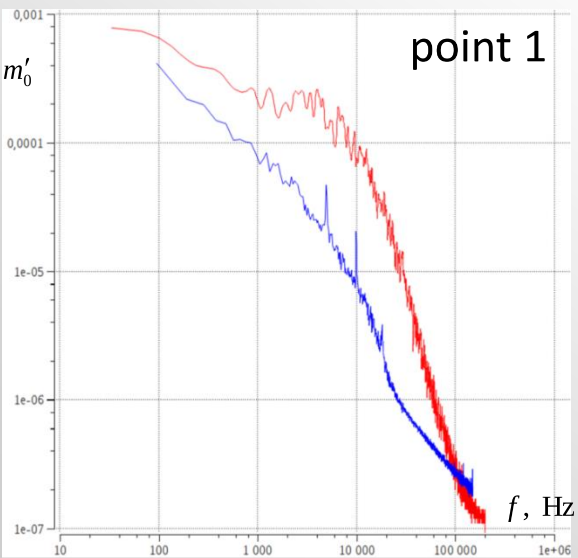

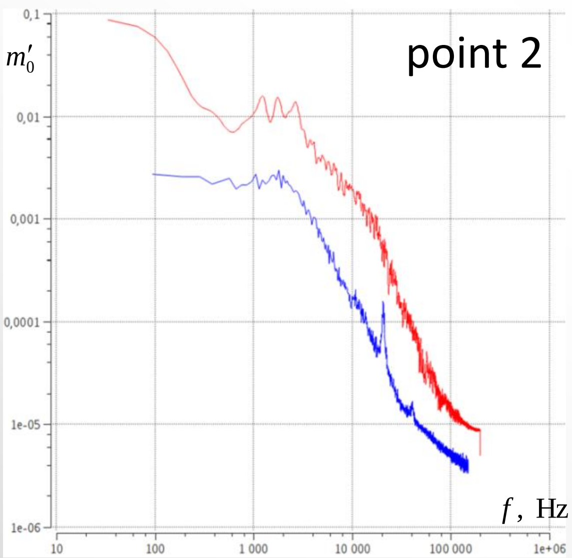

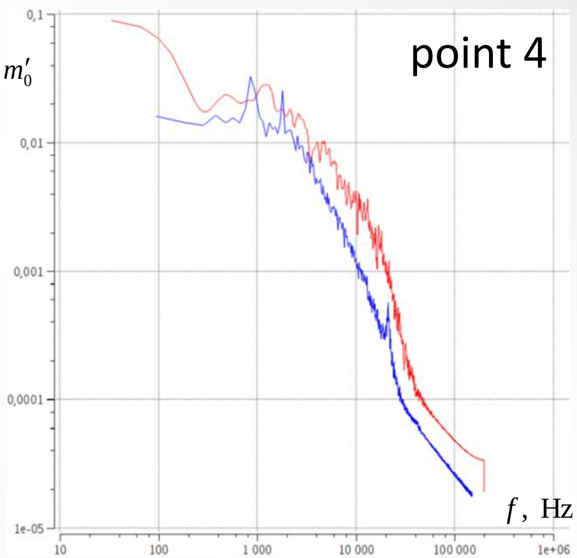

- spectra in shear layer are predicted better than along the centerline

Nozzle test case: mesh and first computations

Inner surface of nozzle (medium mesh)

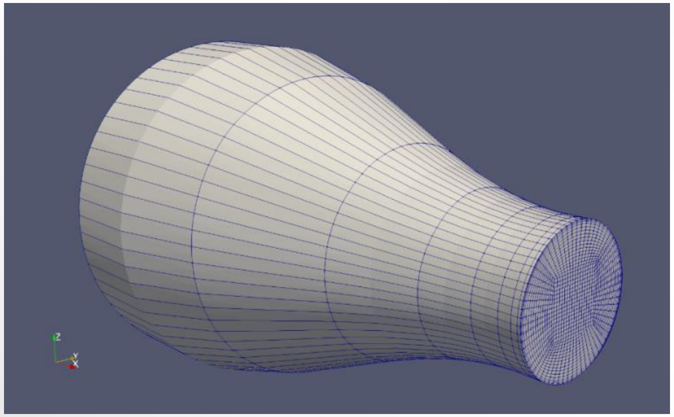

Nozzle tip

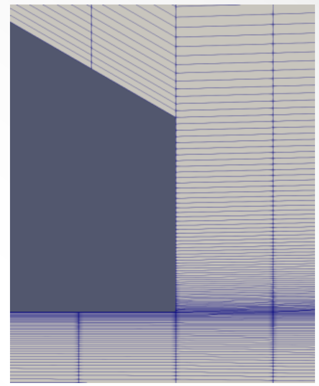

Fine mesh from NASA website

New fine DDES mesh for wall functions

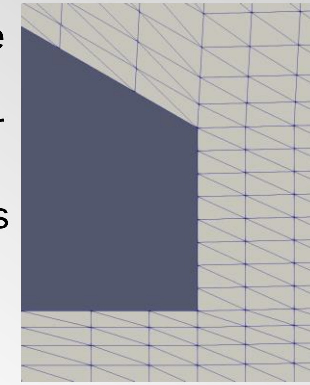

Problems with Discontinuous Galerkin computations

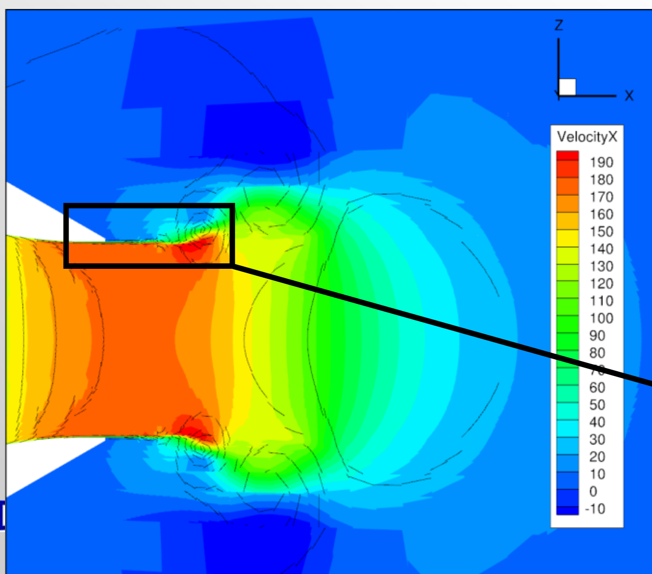

- instability at the origin of the shear layer
- problem is independent of Mach number
- DG monotonization is now considered

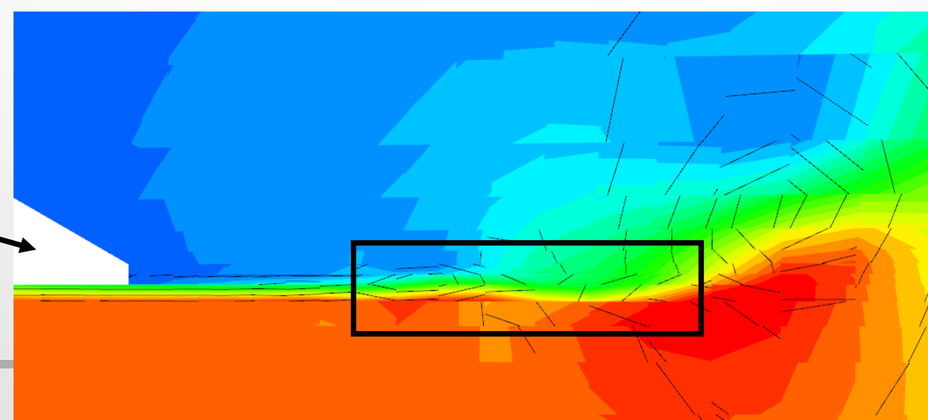

Conclusions

- DG approach up to K=5 have implemented in TsAGI's CFD code successfully;
- To achieve enstrophy error lower than 20% in the Taylor–Green vortex problem, WENO class A scheme requires at least twice more time than high order DG. This difference becomes larger as the required accuracy grows;
- In the computations on a cluster of up to 4000 cores, the speed of the program is increased by more than 1.8 times with each doubling of core number. Use of a biggest number of cores requires a multilevel parallelization involving OpenMP;
- Second order FV RANS and DDES calculations for nozzle test case performed. For high-order DG calculations of nozzle limiting procedure is required;